This is the peer-reviewed, final accepted version for American Mineralogist, published by the Mineralogical Society of America.
The published version is subject to change. Cite as Authors (Year) Title. American Mineralogist, in press.
DOI: https://doi.org/10.2138/am-2021-7670. http://www.minsocam.org/

Timescales of crystal mush mobilization in the Bárðarbunga-Veiðivötn volcanic system based on olivine diffusion chronometry

Alberto Caracciolo[1,2], Maren Kahl[3], Enikő Bali[1,2], Guðmundur H. Guðfinnsson[1], Sæmundur A. Halldórsson[1], Margaret E. Hartley[4]

(1) Nordic Volcanological Center, Institute of Earth Sciences, University of Iceland, Sturlugata 7, 101 Reykjavík, Iceland.
(2) Faculty of Earth Sciences, University of Iceland, Sturlugata 7, 101 Reykjavík, Iceland.
(3) Institut für Geowissenschaften, Universität Heidelberg, Heidelberg, Germany
(4) Department of Earth and Environmental Sciences, University of Manchester, Manchester, UK

*Corresponding author
Alberto Caracciolo
Tel. +354 7794573
Email: alc10@hi.is

Abstract

This is the peer-reviewed, final accepted version for American Mineralogist, published by the Mineralogical Society of America.
The published version is subject to change. Cite as Authors (Year) Title. American Mineralogist, in press.
DOI: https://doi.org/10.2138/am-2021-7670. http://www.minsocam.org/

The timescales of magmatic processes within a volcanic system may be variable over a volcano's geological history. Crystals reflect environmental perturbations under which they grew, and compositional gradients quenched inside crystals on eruption can be exploited to extract timescales of magmatic processes. Here, we use multi-element diffusion chronometry in olivine macrocrysts to recover their residence time in a melt which ultimately erupted at the surface. The macrocrysts were mobilized by the carrier melt from mushy layers in the magma reservoir, and diffusion timescales likely reflect the time interval between mush disaggregation, ascent and eruption. To unravel the evolution of mush disaggregation timescales with time, we target early-Holocene, middle-Holocene and historical magmatic units erupted in the Bárðarbunga-Veiðivötn volcanic system in Iceland's Eastern Volcanic Zone. Macrocryst contents vary between samples; early-Holocene samples are highly phyric (10-45 vol% macrocrysts) and contain gabbroic nodules, whereas middle-Holocene (5-15 vol%) and historical units (5-10 vol%) tend to be generally less phyric. Early-Holocene olivine macrocrysts have core compositions in the range Fo_{84-87}, whilst middle-Holocene and historical samples record a wider range in core compositions from Fo_{80} to $Fo_{86.5}$. Olivine rims are in chemical equilibrium with their carrier liquid, and are slightly more evolved in early-Holocene units (Fo_{76-81}) compared to middle-Holocene (Fo_{78-80}) and historical (Fo_{81-83}) units. Diffusion chronometry reveals that the timescale between mush disaggregation and eruption has changed over time, with timescales getting shorter approaching recent times. Early-Holocene olivine macrocrysts dominantly record Fe-Mg diffusion timescales between 200-400 days, whilst middle-Holocene and historical units typically record timescales of about 70 and 60 days, respectively. Barometric studies suggest that melts and crystals are likely stored and gradually transferred throughout an interconnected multi-tiered system that ultimately culminate in a mid-crustal reservoir(s) at about 6.8-7.5 ± 2.5 km depth, where final disaggregation by the carrier liquid took place. We argue that, as a result of extensional processes enhanced by rifting events, well-mixed melts got drawn into mid-crustal reservoir(s) causing crystal mush loosening and mobilization. In addition, we propose that more energy in the form of heat and/or melt supply was required in the early Holocene to break up the dense mush fabric and convert it into an eruptible magma. Conversely, as evidenced by the diverse macrocryst content of the historical units and by the lack of gabbroic nodules, the system has become characterized by a less compact mush fabric since at least the middle-Holocene, such that fresh injection of melt would easily loosen and mobilize the mush, resulting in an eruption within a couple of months. This study provides evidence that along axial rift settings, rifting-related processes can help to "pull the mush apart" with no requirement for primitive magma injection as an eruption trigger. Furthermore, we provide evidence that in the Bárðarbunga-Veiðivötn volcanic system specifically, the time between mush disaggregation and eruption has decreased considerably with time, indicating shorter warning times before imminent eruptions.

1. INTRODUCTION

Understanding the time and duration of magmatic processes has been a central topic in volcanology, as time is a critical parameter to assess volcanic risk (Sparks and Sigurdsson 1977). Great strides have been made over the past decades in developing diffusion chronometry as a fundamental tool to retrieve time information of magmatic processes recorded in minerals (Martin et al. 2008; Costa and Morgan 2010; Kahl et al. 2011, 2013, 2015, 2017; Ruprecht and Plank 2013; Cooper and Kent 2014; Viccaro et al. 2016; Hartley et al. 2016; Dohmen et al. 2017; Mutch et al. 2019a, 2019b).

The chemistry of igneous minerals reflects the environment(s) under which they grew, and any perturbation of pressure, temperature, melt composition or oxygen fugacity might be recorded by their composition (Ginibre et al. 2007; Blundy and Cashman 2008; Streck 2008). Changing growth conditions result in chemical zoning in minerals. At magmatic temperatures, compositional gradients tend to be smoothed out via diffusion as long as the system stays above the closure temperature. Diffusion chronometry is used to model the re-equilibration of different elements across compositionally distinct zones in crystals to derive the time that elapsed between the onset of the perturbation in growth conditions (e.g. magma injection) and the point at which diffusion effectively ceased to play a significant role (e.g. volcanic eruption) (Turner and Costa 2007; Costa et al. 2008; Costa and Morgan 2010; Dohmen et al. 2017). Diffusion chronometry in plagioclase, olivine and pyroxene crystals has been widely applied to estimate timescales of mixing processes and recharge events (Costa and Chakraborty 2004; Kahl et al. 2011, 2015; Ruprecht and Cooper 2012; Chamberlain et al. 2014; Rae et al. 2016; Viccaro et al. 2016; Rasmussen et al. 2018), magma ascent rates (Demouchy et al., 2006; Hartley et al., 2018; Mutch et al., 2019a; Ruprecht and Plank, 2013), cooling rates (Coogan et al. 2005; Faak et al. 2013; Sio et al. 2013; Newcombe et al. 2014) and crystal mush disaggregation timescales (Costa et al. 2010; Cooper and Kent 2014; Moore et al. 2014; Hartley et al. 2016; Pankhurst et al. 2018; Nikkola et al. 2019; Mutch et al. 2020).

In Iceland, magma storage bodies occur over a large range of depths (Neave et al. 2013; Haddadi et al. 2017; Neave and Putirka 2017; Hartley et al. 2018; Caracciolo et al. 2020) and understanding the rate of magma transfer between the different active storage zones in such active magmatic systems is vital for the interpretation of signals of volcanic unrest. The 2010 Eyjafjallajökull eruption provided a significant step forward in linking petrological and geophysical data: pre-eruptive geophysical signals (e.g. ground displacement and earthquake frequency) (Sigmundsson et al. 2010) registered between November 2009 and March 2010 are consistent with the onset of magma injection in the Eyjafjallajökull system obtained through diffusion chronometry on zoned olivine crystals (Pankhurst et al. 2018).

Diffusion chronometry applied to recent Icelandic eruptions indicates very short timescales of magma mixing (Viccaro et al. 2016) and crystal mush disaggregation (Hartley et al. 2016; Pankhurst et al. 2018; Nikkola et al. 2019) beneath Icelandic volcanoes. However, these studies mainly focus on recent and single eruptions in different volcanic systems and it is still unknown whether timescales of magmatic processes are uniform within the lifespan of a single volcanic system. Here we employ diffusion chronometry by modeling the diffusive relaxation of Fe-Mg, Mn and Ni in olivine macrocrysts to retrieve timescales of crystal mush disaggregation beneath the Bárðarbunga-Veiðivötn volcanic system in central Iceland. Secondly, we merge diffusion modeling results with prior geobarometric constraints in order to reconstruct magmatic processes in the Bárðarbunga-Veiðivötn volcanic system throughout the Holocene. To do this, we have targeted well-characterized magmatic units of different age (early-Holocene to historical) within the same volcanic system. We determine the time that has elapsed between magma injection into the crystal mush reservoirs and the subsequent eruption, and importantly, we discuss how these timescales have changed over the Holocene period.

2. GEOLOGICAL BACKGROUND, SAMPLE LOCALITIES AND PREVIOUS WORK

Iceland is the only place in the world where a mid-ocean ridge intersects a mantle plume directly. The on-land manifestation of the Mid-Atlantic Ridge is split into four main neovolcanic rift zones (Fig. 1a), the Reykjanes Volcanic Belt (RVB), the Western Volcanic Zone (WVZ), the Eastern Volcanic Zone (EVZ) and the Northern Volcanic Zone (NVZ). The Bárðarbunga volcanic system is the largest volcanic system of the EVZ and it rises above the current presumed centre of the mantle plume (Bjarnason 2008) (Fig. 1a). The southwesternmost segment of the Bárðarbunga volcanic system is commonly referred to as the Bárðarbunga-Veiðivötn volcanic system and it consists of a fissure swarm that fades out towards the south into the Torfajökull volcanic system (Thordarson and Larsen 2007; Larsen and Guðmundsson 2014).

The volcanic units in the Bárðarbunga-Veiðivötn volcanic system considered in this study are represented by a suite of well-characterized samples, which have previously been studied by Caracciolo et al. (2020). Here we summarize key findings of that study and we guide the reader to this work for further details on these units and the geology of the area. The sampled units are: Brandur, Fontur and Saxi (early Holocene), Þjórsárdalshraun and Drekahraun (middle Holocene) and Veiðivötn 1477 (historical) (Fig. 1b). Brandur, Fontur and Saxi are three early-Holocene tephra cones and the samples consist of fresh, macrocryst-rich, glassy tephra material and highly crystalline gabbroic nodules. Þjórsárdalshraun and Drekahraun are dated as middle-Holocene units (3-4 ka, Pinton et al. 2018) and the samples come from lava and fresh vesicular scoria, respectively. Veiðivötn 1477 was produced in a 65 km long fissure eruption that occurred in 1477 AD (Fig. 1b). Caracciolo et al. (2020) found that all samples contain macrocrysts and polymineralic clots, indicative of a crystal mush origin. The compositions of the macrocrysts vary with time, with early-Holocene magmatic units containing more

This is the peer-reviewed, final accepted version for American Mineralogist, published by the Mineralogical Society of America.
The published version is subject to change. Cite as Authors (Year) Title. American Mineralogist, in press.
DOI: https://doi.org/10.2138/am-2021-7670. http://www.minsocam.org/

primitive compositions compared to middle-Holocene and historical magmatic units. Application of different thermobarometers to crystals, groundmass glasses and melt inclusions (MIs) revealed temporally invariant crystallization conditions in the middle crust, at about 1.9-2.2 kbar (6.8-7.8 km), along with the occurrence of deep-seated storage reservoir(s) during the time covered by the oldest magmatic units. This deep crystallization record has been linked to a different crustal response associated with post-glacial isostasy rebound (Gee et al. 1998; Sinton et al. 2005; Le Breton et al. 2016).

3. SAMPLE PREPARATION AND ANALYTICAL METHODS

Unaltered olivine macrocysts in the size range 0.5-2.4 mm were hand-picked from crushed tephra and lava samples and mounted in epoxy resin to expose a flat surface. High-contrast backscattered electron (BSE) images were taken of olivines using the JEOL JXA-8230 SuperProbe electron probe microanalyzer (EPMA) at the Institute of Earth Sciences, University of Iceland. ImageJ software was used to process the BSE images to identify crystals with zoning patterns and to select traverses suitable for diffusion modeling.

3.1. Electron microprobe analyses (EMPA)

Olivine concentration profiles of major and minor elements (Si, Ti, Al, Cr, Fe, Mn, Ni, Mg, Ca) were acquired using the EPMA at the University of Iceland. Chemical transects were measured using a focused beam with an accelerating voltage of 15 kV and a probe current of 20 nA. A counting time of 30 s at the peak and background was used for Ti, Al, Mn, Cr and Ni. Si, Fe, Mg and Ca were analyzed using a counting time of 30 s at peak and 15 s at the background. Chemical profiles with point spacing between 3-6 μm (25 to 100 points) were measured perpendicular to macrocryst margins along different directions in a total of 121 olivine grains from all studied eruptive units. Multiple standard samples were analyzed prior to and after each session. Error bars reported in the chemical diagrams indicate 2σ of multiple standard analyses ($2\sigma_{Fo}$=0.34 mol%, $2\sigma_{Mn}$=0.038 wt%, $2\sigma_{Ni}$=0.018 wt%). In order to test for equilibrium conditions, groundmass glasses immediately around olivine macrocrysts were analyzed with the EPMA. In this study, we include some olivine-hosted MIs (n=8) analyzed by Caracciolo et al. (2020), along with new MI data (n=13) (supplementary material S1). See Caracciolo et al. (2020) for analytical details about MI analyses and post-entrapment process correction.

3.2. Electron backscatter diffraction (EBSD)

Crystallographic orientations of olivine macrocrysts were obtained using electron backscatter diffraction (EBSD; Prior et al., 1999; Costa and Chakraborty, 2004) on the FEI Quanta 650 FEG-SEM at the University of Leeds Electron Microscopy and Spectroscopy Centre (LEMAS). Characterizing the crystallographic directions in olivine with respect to the micro-analytical traverses is essential for accurate diffusion modeling, as the diffusivity of different elements (e.g. Fe–Mg or Ni) in olivine is strongly anisotropic, with diffusion along the c-axis being six times faster than that along the a- and b-axes (e.g. Clark and Long 1971; Dohmen et al. 2007).

To minimize uncertainty in the determination of the orientation data, orientation maps consisting of hundreds of EBSD point determinations were conducted for each macrocryst (Kahl et al., 2017). Maps were acquired using an accelerating voltage of 20 kV and a spot size of 5.5 µm. EBSD maps over crystal areas of interest were generated and processed using the HKL CHANNEL5 EBSD post-processing software, enabling the extraction of hundreds to thousands of orientation measurements. Measured Euler angles were converted into trends and plunges of the olivine crystallographic a-, b- and c-axes using Stereo32 software developed at the Ruhr-Universität Bochum. Using this software, it is possible to calculate the angles between the measured electron microprobe traverses and the crystallographic a-, b- and c-axes in olivine (Supplementary material S2) (Costa and Chakraborty 2004; Kahl et al. 2011).

4. KINETIC MODELING

At high temperatures, compositional heterogeneities in magmatic crystals will homogenize due to diffusive relaxation. Following the modeling approach outlined in Kahl et al. (2011, 2013) and Costa and Chakraborty (2004), we modeled the diffusive relaxation of Fe-Mg, Ni and Mn zoning in olivine macrocrysts from all studied localities. Details of the methods and the criteria for the choice of concentration profiles for modeling, including tests for robustness, have been reported in full detail by Costa et al. (2008) and Kahl et al. (2011, 2013).

Among 121 olivine grains representing all eruptive units (Table 1), 21 grains show dipping plateaux (Shea et al. 2015) or zoning patterns probably related to crystal growth (Costa et al. 2008). These grains are not suitable for olivine diffusion modeling and were excluded from further consideration. For the diffusion models, the spacing was set to 5µm, which is a good compromise between calculation speed and EMPA resolution of the analyzed diffusion profiles. For each crystal, the modelling curves were calculated by manually changing the number of time steps until a best-fit curve for a given Fe-Mg diffusion profile was observed. Therefore, depending on the zonation pattern, the number of time steps was different for each crystal. Subsequently, we used the same number of time steps and the identical initial conditions to model diffusion profiles of Mn and Ni (Fig. S1.4). In most of the cases, best-fit curves (and comparable timescales) were observed for Fe-Mg, Mn and Ni (Fig. S1.4), suggesting that zoning profiles are likely to be controlled by diffusion.

4.1. Modeling approach

This is the peer-reviewed, final accepted version for American Mineralogist, published by the Mineralogical Society of America.
The published version is subject to change. Cite as Authors (Year) Title. American Mineralogist, in press.
DOI: https://doi.org/10.2138/am-2021-7670. http://www.minsocam.org/

We used the composition-dependent, one-dimensional expression of the diffusion equation (i.e. Fick's second law):

$$\frac{\partial C_i(x,t)}{\partial t} = \frac{\partial}{\partial x}(D_i \frac{\partial C_i(x,t)}{\partial x})$$

where C_i is the concentration of element i, x denotes the distance, D_i is the diffusion coefficient of element i, and t is time. The evolution of the concentration with time (t) at different spatial coordinates (x), $C_i(x,t)$, is obtained numerically using a one-dimensional finite difference scheme (see Costa et al. 2008). In this study, we mainly focused on Fe-Mg but also on Ni and Mn zoning when possible, to increase the robustness of the calculated timescales. Diffusion coefficients are functions of pressure, temperature, composition, oxygen fugacity and crystallographic orientation, and were taken from experimentally determined data (Fe–Mg and Mn: Dohmen et al., 2007; Ni: Petry et al., 2004 and Holzapfel et al., 2007).

4.2. Modeling parameters and error propagation

4.2.1. Initial and boundary conditions

The initial condition refers to the shape of the zoning pattern before diffusive modification. The strategies outlined in Kahl et al. (2011) were adopted to identify initial conditions for each profile. In most cases, we assumed a homogeneous initial profile (Fig. S1.1a), guided by the occurrence of extended compositional core plateaux. Only in a few cases, plateaux at the rims (Fig. S1.1b) were observed. These were interpreted as stranded diffusion profiles and a stepped initial profile shape was invoked.

In our modeling, we assume that macrocrysts re-equilibrated with their host liquid (i.e. open boundary conditions) and that the composition of the liquid is constant with time within a specific magmatic unit.

4.2.2. Input parameters

Clinopyroxene-liquid, OPAM and liquid-only thermobarometry constraints suggest that the final equilibration depth of the carrier liquids before eruption and olivine rim crystallization occurred in the mid-crust at about 1.1-2.7 kbar pressure, at temperatures of 1160-1175 °C (Caracciolo et al. 2020). Therefore, we have modeled the chemical zoning with temperature and pressure set according to the magmatic unit under consideration (Caracciolo et al. 2020). A summary of input temperature and pressure conditions is reported in Table 1. Oxygen fugacity was set to the FMQ (Fayalite-Magnetite-Quartz) buffer based on spinel-olivine oxybarometry.

4.2.3. Error propagation

Timescale uncertainties have been calculated following the method described by Kahl et al. (2015), with temperature showing the largest effect on the propagated error. For instance, a 1σ temperature uncertainty of ± 5 °C yields errors of ± 134 days for a calculated diffusion timescale of 1000 days, ± 13.4 days for a timescale of 100 days and ± 1.4 days for a timescale of 10 days.

5. RESULTS

5.1. Petrography of the samples

Among all studied samples, plagioclase is the principal macrocryst (>0.5 mm) phase, followed by olivine and clinopyroxene. Early-Holocene units consist of tephra and high-crystallinity gabbroic nodules. Tephra are slightly vesicular (~15-20 %) and contain between ~15 and ~45 vol% macrocrysts (Fig. 2a). Nodules (Fig. 2b) consist of pseudo-spherical olivine gabbros (up to 10 cm in diameter) with a

This is the peer-reviewed, final accepted version for American Mineralogist, published by the Mineralogical Society of America.
The published version is subject to change. Cite as Authors (Year) Title. American Mineralogist, in press.
DOI: https://doi.org/10.2138/am-2021-7670. http://www.minsocam.org/

crystallinity between ~80-95%, and they are made of a network of plagioclase macrocrysts (~80-85%), interspersed with olivine macrocrysts (~5-10%), clinopyroxene (~5%) and interstitial glass (~5-10%) (Fig. 2 b-c). Olivine crystals found in the gabbroic nodules are morphologically and texturally similar to those found in the tephra samples. Lava and scoria samples from middle-Holocene units show variable vesicularity (50-80 %) and a low abundance of macro- and microcrysts (Fig. 2d). The macrocryst content ranges between ~5-15 %, with plagioclase macrocrysts being more abundant than olivine and clinopyroxene (Fig. 2d). Historical samples consist of fresh, highly vesicular (~70-90 %), crystal-poor scoria with the most crystalline samples having ~5-10 % macrocrysts. Detailed sample petrography is provided by Caracciolo et al. (2020).

5.2. Olivine - chemistry and zoning

We have measured a total of 173 chemical profiles in 121 olivine macrocrysts from all localities (Table 1). The olivine core and rim compositions range between Fo_{76-87} and Fo_{74-84} [Fo=100*Mg/(Mg + Fe), in mol%], respectively, although we find systematic compositional differences between eruptions (Fig. 3).

Brandur, Fontur and Saxi olivine macrocryst cores record the smallest compositional variation, whilst rims show the largest range among all magmatic units (Fig. 3a). Olivine cores from Brandur are in the range $Fo_{84.5-86.5}$ and rims in the range Fo_{77-81}. Fontur olivines have core and rim compositions of $Fo_{83.5-87.5}$ and $Fo_{76-80.5}$, respectively. Saxi olivine macrocrysts preserve cores of $Fo_{85-86.5}$ and rims of $Fo_{77.5-79}$. Olivine cores from Fontur and Saxi gabbroic nodule samples display a larger Fo range ($Fo_{80-87.5}$) than olivine cores in tephra samples (Fo_{85-87}) (Fig. S1.2). Brandur olivines record remarkably homogeneous core compositions within gabbroic nodule and tephra samples, with 1 mol% difference between the two. Most of the tephra olivines from Brandur are slightly more primitive ($Fo_{\sim 86}$) than nodule olivines

DOI: https://doi.org/10.2138/am-2021-7670. http://www.minsocam.org/

($Fo_{\sim 85}$) (Fig. S1.2), although this difference is not observed in Fontur and Saxi. Drekahraun and Þjórsárdalshraun record similar olivine core composition range ($Fo_{80-85.5}$), while olivine rims are in the range Fo_{75-81} and Fo_{81-83}, respectively (Fig. 3a). Olivine macrocrysts from the Veiðivötn 1477 eruption display core compositions in the range $Fo_{80-86.5}$ and rims in the range Fo_{78-81}. The majority of olivine macrocrysts display normal zoning (Fig. 3a and Fig. S1.1a), with forsterite-rich cores surrounded by less forsteritic rims. Two macrocrysts from Veiðivötn 1477 and one macrocryst from Drekahraun display reverse zonation (Fig. 3a and Fig. S1.1b), with the latter showing a strong compositional gradient between core (Fo_{76}) and rim (Fo_{82}). Some olivine macrocrysts from Drekahraun (n=4), Þjórsárdalshraun (n=3) and Veiðivötn 1477 (n=9) show complex zoning patterns with reversely zoned macrocryst interiors followed by normally zoned outermost rims (Fig. S1.1c). The difference in Fo content between the core and the intermediate zone is always lower than 1 mol% but still above the analytical uncertainty ($2\sigma_{Fo}$= 0.34). This intermediate pattern is not recorded by other elements. Finally, we do not observe any unzoned olivine macrocrysts in the magmatic units discussed in this work (Fig. 3a).

At any given Fo content, olivine cores from early-Holocene, middle-Holocene and historical units do not show any difference in terms of Mn and Ni. Primitive olivine cores (Fo_{85-87}) from early-Holocene samples have Mn contents in the range 1400-1700 ppm and Ni contents in the range 1200-1700 ppm. Less primitive (Fo_{78-82}) olivine cores are found in the historical samples and they record Mn contents between 2000-2500 ppm and Ni contents between 800-1300 ppm. The measured Mn and Ni contents overlap with those of olivine macrocrysts from the 2014-15 Holuhraun eruption (Halldórsson et al. 2018) (Fig. S1.3).

5.3. Relation to the carrier liquid

Each eruptive unit is characterized by a specific range in groundmass glass compositions (Fig. 3b), which is assumed to represent the carrier liquid composition. Early-Holocene groundmass glasses have the largest chemical variability (MgO 5.5-7.5 wt%, TiO_2 1.0-2.5 wt%), whereas recent units are more homogeneous (Caracciolo et al., 2020). Middle-Holocene carrier liquids have MgO and TiO_2 contents in the range 7.0-7.5 wt% and 1.6-1.8 wt% respectively, while historical carrier liquids are in the range 6.3-6.9 wt% for MgO and 1.6-2.0 wt% for TiO_2. The melt Mg# (Mg#= 100*Mg/(Mg+Fe^{2+})) of the carrier liquid was obtained by calculating Fe^{2+} and Fe^{3+} contents following the model of Kress and Carmichael (1991) at the FMQ buffer. Following this procedure, 91% of olivine macrocryst rims are in chemical equilibrium with the carrier liquid (Fig. 3b).

5.4. Diffusion modeling results

We modeled 100 olivine crystals with zoning patters related to diffusive relaxation of Fe and Mg and well-suited for diffusion modelling (Fig. 4). Independent Fe-Mg timescale results for each locality are reported in Fig. 5 and in S1, while a summary is listed in Table 1. Kernel density estimate (KDE) distribution curves are shown in Fig. 6.

5.4.1. Brandur, Fontur and Saxi (early-Holocene)

Olivine macrocrysts from the three tephra cones, Brandur, Fontur and Saxi, record a large range of timescales, varying from 20 to 1330 days (Fig. 5a-c and Fig. 6a). The large range of timescales is observed both, in olivines found in gabbroic nodules and in tephra samples (Fig. 5a-b). KDE distribution curves largely overlap (Fig. 6a), with the majority of olivines (63%) recording timescales between 150 and 400 days (0.4-1.1 years). Only 17% of the olivines give timescales shorter than 150 days and 20% longer than 400 days. Brandur olivines (n=29) show a narrowly focused major peak at 340 days. Fontur olivines (n=16) display the widest timescale distribution, with a major peak located at 444 days and a large shoulder with timescales between ~100 and ~230 days (n=5). The shortest timescale of 19 days is recorded by one macrocryst from Fontur (Fig. 5b). Finally, Saxi olivines (n=11) show most probable timescales of 210-350 days (Fig. 6a), with a main peak at 220 days, and a minor band located at a timescale >800 days (n=2).

5.4.2. Þjórsárdalshraun and Drekahraun (middle-Holocene)

Diffusion timescales calculated for Þjórsárdalshraun olivines show a scattered KDE distribution (Fig. 6b). Timescales are all below 110 days (Fig. 4d), with a major peak at 24 days. However, the Þjórsárdalshraun samples come from a section of the lava that had flowed about 50-60 km before ultimately forming a rootless cone field. For this reason, olivines from this unit are likely affected by post-eruptive diffusion and/or crystallization processes and timescale results are treated with caution. Indeed, only a few macrocrysts (n=7) suitable for diffusion measurements were found within the Þjórsárdalshraun samples and sample bias might affect the distribution. In contrast, samples from the Drekahraun unit consist of fresh scoria. KDE timescale distribution for Drekahraun olivines show a prominent peak at 78 days and a minor peak at 30 days (Fig. 5e and Fig. 6b). Only one macrocryst records a timescale above 100 days (118 days). Intermediate zoning patterns observed in some middle-Holocene macrocrysts were modeled sequentially and return diffusion timescales between 2-29 days.

5.4.3. Veiðivötn 1477 (historical)

83% of olivine macrocrysts from Veiðivötn 1477 register diffusion timescales shorter than 100 days (Fig. 5f), with a main peak in the KDE distribution at 55 days (Fig. 6c). A minor peak is observed at 15 days, while only 4 macrocrysts out of 22 record timescales longer than 100 days (Fig. 5f). Finally, the intermediate chemical zoning found in some macrocrysts gives an average timescale of 25 days.

6. DISCUSSION

6.1. Relationship between melt composition, magma depth and timescales

Barometry constraints show that the carrier liquid last equilibrated with the crystal cargo in a reservoir(s) located in the middle-crust (7-11 km depth), before being erupted (Caracciolo et al. 2020). The cores of 21 olivine macrocrysts contain large (up to 120 µm in diameter), naturally quenched melt inclusions (e.g. Fig. 4g and Fig. S1.4i), which are mostly hosted in early-Holocene units (Fig. 7a). These melt inclusions have MgO contents between 7.6 and 9.2 wt% and TiO_2 in the range 0.8-1.8 wt% (Mg#55-65). We estimated MI equilibration pressures within the Bárðarbunga-Veiðivötn plumbing system by applying the Olivine-Plagioclase-Augite-Melt (OPAM) barometer (Yang et al. 1996; Hartley et al. 2018) with the goal to locate the macrocrysts within the crust. MI equilibration pressures (n=3) of middle-Holocene and historical samples range between 1.8 and 1.9 kbar (Fig. 7a) and they are hosted in olivine cores with compositions in the range $Fo_{81.6-84.6}$. However, MIs hosted in plagioclase macrocrysts record pressures down to 4 kbar (Caracciolo et al. 2020). Early-Holocene units register a much larger pressure variation, between 1.5 and 6 kbar, with a clear positive relationship between olivine composition, MI composition and MI equilibration pressure (Fig. 7a). The olivine crystals become more evolved as MI equilibration pressures decrease, with primitive olivines (Fo>86) recording the highest pressures (4-6 kbar) and the most primitive MI compositions (Mg# 64-65) (Fig. 7a). These findings, which are in good agreement with the data of Caracciolo et al. (2020), support a stacked-sills model (Kelemen et al. 1997; Maclennan 2019) in which olivine macrocrysts are exposed to slightly more evolved environments as they move shallower in the crust (Fig. 8).

The shortest diffusion timescales (6-108 days) are recorded by macrocrysts from middle-Holocene and historical units, which likely crystallized at mid-crustal (7-11 km) levels (Fig. 7b and Caracciolo et al. 2020). In contrast, early-Holocene olivines cluster at timescales between 200-400 days (Fig. 7b) and they most likely crystallized throughout the crustal section. Although there is a positive correlation between early-Holocene olivine depths and their compositions (Fig. 7a), we do not observe any clear relationship between MI equilibration pressure and olivine diffusion timescales (Fig. 7b) nor between olivine Fo content and diffusion timescales (Fig. S1.5). This suggests that olivine macrocrysts are likely to have been transported up to mid-crustal (7-11 km) mush piles during earlier remobilization events throughout a multi-tiered system of interconnected stacked sills in which crystals are gradually transported to higher levels until they accumulate in the main mid-crustal reservoir at about 7-11 km. Indeed, the absence of intermediate zoning sectors may indicate that these macrocrysts resided in the mid-crust for a period sufficiently long to erase any chemical gradient previously formed. Eventually, at some point in the early-Holocene, injection of melts with variable composition (Caracciolo et al. 2020) into the mid-crustal reservoir(s) caused remobilization of these deep-origin olivines and their incorporation in the carrier melt.

6.2. Timing of crystal mush disaggregation and triggering mechanism

Gabbroic nodules found in early-Holocene magmatic units are unique samples whose mineralogical and textural characteristics indicate that they represent exhumed pieces of the crystal mush (Hansen and Grönvold 2000; Caracciolo et al. 2020). The lack of notable chemical differences between olivines in the gabbroic nodules and in the tephra samples (Fig. S1.2) support their common origin. Except for Brandur samples (Fig. S1.2), no notable differences in composition are observed between olivines coming from the mush and olivines carried in the melt as a result of disaggregation processes (Fig. 5a-c). While the majority of olivine rim compositions are found to be in chemical equilibrium with the carrier liquid (Fig. 3b), olivine cores are not. They most likely crystallized from a set of compositionally diverse primitive melts, as supported by MI data (Caracciolo et al. 2020). In most cases, olivine cores are homogenous, forming long compositional plateaux, which can extend up to 200 µm within the largest grains (Fig. 4b, h). This observation suggests long residence time whereby olivine cores have either been re-equilibrated completely through diffusion or they have grown in a reservoir(s) under steady chemical and physical conditions before rim crystallization occurred. In contrast, some olivine cores in the more recent samples (middle-Holocene and historical) record more complex zoning patterns, with Fo variations of ~1 mol% (Fig. S1.1c). These jumps likely relate to changes in the intensive thermodynamic variables (composition, pressure, temperature and/or oxygen fugacity) of the magmatic environment (e.g. Kahl et al. 2017), so that the next increment of olivine that grew had a slightly different composition.

The decrease in the Fo content at the rims is an evidence for changes in the chemical and or physical conditions of the reservoir. We infer that the outermost normal zoning is related to interaction of a relatively evolved melt (e.g. the final carrier liquid) within an undisturbed crystal mush reservoir(s); the evolved liquids got injected into the reservoir and permeated the mush, thereby starting the diffusion clock after efficient mixing was achieved (Fig. 8). This process most likely caused disaggregation of mush clots and addition of mush crystals (Sigmundsson et al. 2020) into the carrier melt. If this is the case, then diffusion timescales correspond to the time elapsed between the disaggregation of crystal mush following magma injection, when chemical re-equilibration with the

DOI: https://doi.org/10.2138/am-2021-7670. http://www.minsocam.org/

carrier liquid started, and the eruption, when diffusion ceased to play a role (Fig. 8). Specifically, the composition of the tholeiitic basalt magma being injected into the mush reservoir has not remained constant over the Holocene period (see 5.2 above and Fig. 1. in Caracciolo et al. 2020).

Olivine macrocrysts with complex and reverse zoning patterns are widespread in off-rift Icelandic settings and their zoning features have been associated with late mafic magma replenishment events (e.g. Mattsson and Oskarsson 2005; Pankhurst et al. 2014; Viccaro et al. 2016), which could have triggered the eruptions. In contrast, rift-related olivine macrocrysts commonly preserve normal zoning patterns (e.g. Neave et al. 2013, 2015; Thomson and Maclennan 2013; Hartley et al. 2016; Halldórsson et al. 2018), which could indicate a different triggering mechanism. In fact, about 95% of the olivine macrocrysts studied in this work do not preserve direct evidence for late mafic recharge events. It is possible that slightly deeper, well-mixed and relatively evolved melts pockets could get remobilized and intrude the mid-crustal reservoir as a result of rift-related events that would "pull the mush apart", promoting mush disaggregation and the vertical rearrangement of crystal and melt layers within the crust. If so, rifting-related events can play a fundamental role on eruption triggering mechanisms along axial rift zones.

6.3. Temporal variation of crystal mush disaggregation timescales in the Bárðarbunga-Veiðivötn volcanic system

The older Holocene macrocrysts appear to have resided longer in their carrier liquid than the younger macrocrysts (Fig. 6 and S1.5). One noteworthy observation is that early-Holocene units contain mush nodules and a larger macrocryst load than the younger units (Fig. 2 and Fig. 9). The gabbroic nodules contain up to 90 vol% macrocrysts and confirm the existence of a crystal-rich mush fabric. In Fig. 9 we show diffusion modeling timescales yielded by olivine macrocrysts in relation to the estimated macrocryst content of the samples for each studied time period. We also report diffusion durations for the subglacial Skuggafjöll eruption (Mutch et al. 2020) that occurred in the Bárðarbunga-Veiðivötn volcanic system and which shares many features with our samples. The Skuggafjöll products consist of a highly phyric (6-45% by volume), plagioclase-rich basalts (Neave et al. 2014) that crystallized at about 11 ± 4 km (Neave and Putirka 2017). Subglacial and early-Holocene units record the largest timescale spread and the most abundant crystal content (up to 45 vol%). On the other hand, middle-Holocene and historical units preserve a smaller macrocryst content (5-15 vol %) than early-Holocene and subglacial units, which is coupled with much shorter timescales and narrower timescale ranges (Fig. 9). Therefore, we suggest that during subglacial and early-Holocene times the mid-crustal mush network required more time to be converted into an eruptible magma (Cashman et al. 2017) because of the occurrence of a more compact mush fabric. It is possible that multiple injections of melt fractions were needed to eventually mobilize the rigid network of the mush reservoir(s) (Fig. 8a-b), causing long residence times of macrocrysts in the reservoir(s). Furthermore, we find important to highlight that crystals found in the gabbroic nodules and crystals found in the tephra samples reveal the same timescales (Fig. 5). Those units were sourced from packed mush piles, which required more heat or a larger volume of intruding magma to be weakened and mobilized compared to the present. The larger volume of magma or energy (i.e. heat) supply is consistent with the increase of magma production rates observed in Iceland during the early Holocene that were likely caused by glacio-isostacy effects (Sinton et al. 2005; Le Breton et al. 2016; Caracciolo et al. 2020). In contrast, the present-day system is most likely characterized by a less dense mush fabric and a larger melt-mineral ratio (Fig. 8c-d). If this is true, then since the middle-Holocene, injections of smaller melt fractions would be enough to mobilize the mush network almost instantly (Fig. 8d), with magma flowing towards the surface within short timescales. The shortening of timescales approaching the present day is consistent with magma transport durations of about 1-12 days (Fig. 10), estimated for the 2014-15 Holuhraun lava (Hartley et al. 2018) that was emplaced in the northern segment of the Bárðarbunga volcanic system.

6.4. Timescales of magmatic processes in Iceland and MOR settings

Our study is the first to obtain diffusion timescales for a temporally diverse magmatic suite erupted within the same volcanic system (Fig. 10). Our results can be combined with diffusion timescales estimated for the subglacial Skuggafjöll eruption (Mutch et al. 2020) to evaluate the temporal evolution of crystal mush disaggregation from the subglacial period until historical time within the Bárðarbunga-Veiðivötn volcanic system. Diffusion modeling of plagioclase and olivine macrocrysts from Skuggafjöll yield most probable timescales in the range 50-400 days (Mutch et al. 2020), suggesting that mush disaggregation processes started about a year or less prior to the eruption. These estimates are in good agreement with the early-Holocene timescales calculated in this study and consistently longer than middle-Holocene and historical mush disaggregation times (Fig. 10).

To our knowledge, published diffusion chronometry data for Icelandic volcanoes ascribed to crystal mush disaggregation processes only concern single eruptions that occurred in the EVZ. Diffusion kinetic data are available for a subglacial unit erupted in the Bárðarbunga-Veiðivötn volcanic system (Mutch et al. 2020), for the 2014-15 Holuhraun lava flow emplaced in the northern segment of the Bárðarbunga volcanic system (Hartley et al. 2018), for the 1783-84 Laki eruption of the Grímsvötn volcanic system (Hartley et al. 2016) and for the 2010 (Pankhurst et al. 2018) and middle-Pleistocene (Nikkola et al. 2019) Eyjafjallajökull eruptions in the southernmost section of the EVZ. With the exception of Skuggafjöll (Mutch et al. 2020), these studies reveal short diffusion times between mush disaggregation and entrainment prior to eruption, on the order of days up to 1-2 months (Fig. 10). These estimates overlap and are consistent with timescales calculated for middle-Holocene and historical units from the Bárðarbunga-Veiðivötn system (Fig. 10). Eyjafjallajökull is the only system studied so far for which there are timescale estimates available for eruptions of different ages. Timescales between mobilization of mush macrocrysts and eruption of about 10-30 days were calculated for the 2010 Eyjafjallajökull eruption (Pankhurst et al. 2018), in good agreement with mush mobilization times of about 9-37 days estimated for the middle-Pleistocene Eyjafjallajökull units (Nikkola et al. 2019).

At the present, Iceland is the only place above a slow-spreading ridge where numerous timescales of mush crystal entrainment to eruption are available and only very few data exist at fast-, intermediate- and slow-spreading MOR settings (Fig. 10). Timescales between mush disruption and eruption are on the order of few days for the East Pacific Rise (fast-spreading ridge) (Moore et al. 2014) and for the Costa Rica Rift (intermediate-spreading ridge) (Costa et al. 2010), while mush disruption beneath Serocki Volcano (slow-spreading ridge) occurred about 1.5 years before an eruption on the seafloor (Costa et al. 2010). Mush disruption to eruption timescales estimated for slow-spreading MOR settings are consistent with timescales obtained from the oldest units from this work. Overall, most timescales calculated at slow-spreading ridges (Fig. 10) tend to be longer (months to years) than the ones obtained at intermediate and fast spreading ridges (days). The fact that the time between mush disintegration and eruption increases with decreasing spreading rates (Zellmer et al. 2012) is consistent with thickening of the lithosphere and increase in the depth of melt levels at slow-spreading ridges (Wanless and Shaw 2012). However, further geospeedometric work on intermediate- and fast-spreading ridges is required to elucidate whether or not there is spreading-rate control of the mush disaggregation-to-eruption timescales along MOR settings.

7. Implications

Samples studied in this work include crystalline gabbroic nodules that most likely preserve the physical and mineralogical features of the mush itself. We modeled Fe-Mg, Mn and Ni diffusion in olivine crystals from Holocene samples of the Bárðarbunga-Veiðivötn volcanic system in central Iceland to reconstruct crystal residence time in the carrier melt, which we link to the time elapsed between melt injection (i.e. mush disaggregation) and eruption.

One important implication highlighted by our study is that not every magma replenishment event results in an eruption. In the early Holocene, a year or more may have elapsed between initial perturbation of the shallow reservoir(s) and final eruption, but the timescale between perturbation and eruption appears to get shorter approaching the present day. This difference in crystal residence times in the carrier liquid appears to be associated with the occurrence of a much denser and more rigid mush fabric in the early Holocene, which required more energy to be loosened, disaggregated and mobilized. In terms of hazard assessment, this study highlights that the Bárðarbunga-Veiðivötn volcanic system has been responding faster to melt injection as time proceeds, providing less warning between magma injection and eruption. This could possibly indicate the recent establishment of dominant magma transfer routes along which magma can quickly migrate towards the surface. More studies on the temporal evolution of magma transport timescales underneath single volcanic systems are needed to better constrain the behavior of volcanic systems through time, with a direct implication for volcanic hazard assessment, especially in regions where the last known eruption occurred long before the installation of modern volcano monitoring networks.

The crystal cargos in our samples do not record any evidence of late-stage primitive magma replenishment that could have triggered the eruption. This feature is observed also in crystals from other rift settings in Iceland. Primitive melts with different compositions have been supplied to the Bárðarbunga-Veiðivötn system during earlier stages of its magmatic history (Caracciolo et al. 2020), but these magmas are typically homogenized by concurrent mixing and crystallization (Maclennan 2008; Caracciolo et al. 2020) before being injected into the shallow crystal mush reservoir. These processes likely take place in a multi-tiered magmatic system made up of stacked sills in which macrocrysts are gradually transported upwards and exposed to melts that become more evolved as they move toward the mid-crustal reservoir(s). A plausible eruption trigger mechanism is that rifting-associated events can enable the vertical rearrangement of crystal and melt horizons and facilitate ascent of relatively evolved and mixed melt pockets stored a at mid-crustal levels, with no requirement to supply hot and primitive magmas. Our findings have broad implications for the dynamics of magmatic processes operating in axial ridge settings, since we emphasize the possibility that rifting events can significantly control the vertical arrangement of crystal and melt layers.

Acknowledgments

EPMA and EBSD data collection was financed by Landsvirkjun energy company (NÝR-18 – 2018). This research work was financially supported by the University of Iceland Research Fund (Nr: HI17060092). We would like to thank Duncan Hedges, Richard Walshaw and Geoffrey E. Lloyd (University of Leeds) for their help with EBSD analyses and data processing. We are grateful to Sylvie Demouchy for editorial handling, and Thomas Shea and Cliff Shaw for their valuable reviews that significantly improved the quality of the manuscript. The involvement of S. A. Halldórsson was partly in relation to the H2020 project EUROVOLC, funded by the European Commission (Grant 731070). M. Kahl acknowledges support from IRF postdoctoral fellowship grant 152726–051 and funding from the Deutsche Forschungsgemeinschaft (DFG, German Research Foundation) - KA 3532/2-1. M. E. Hartley acknowledges support from Natural Environment Research Council (NERC) grant NE/P002331/1. A MATLAB® code for Fe-Mg, Ni and Mn diffusion can be requested from the authors.

Figure captions

Fig. 1 a) Map of Iceland showing the neovolcanic rift zones outlined with dashed lines, individual volcanic systems in yellow (subglacial parts not shown) and the inferred location of the mantle plume is shown as a dotted circle. b) Hillshade map of the southernmost part of the Bárðarbunga volcanic system with sample localities and eruptive units indicated with different colors. SVB: Snæfellsnes Volcanic Belt; RVB: Reykjanes Volcanic Belt; WVZ: Western Volcanic Zone; MIB: Mid-Iceland Belt; EVZ: Eastern Volcanic Zone; NVZ: Northern Volcanic Zone.

Fig. 2. Macroscopic features of studied samples. a) Thin section image of a lava sample from Brandur tephra cone. Note the occurrence of a nodule-like aggregate made of a large plagioclase (~1 cm) and olivine grains. Macrocrysts are found in a glassy, light brown groundmass. b-c) Macroscopic photo of a crystalline olivine gabbro nodule from Fontur tephra cone. This gabbroic nodule contains around ~90 vol% macrocrysts, most of which are plagioclase (white greasy macrocrysts), followed by olivines (yellow-green macrocrysts) and clinopyroxene (dark green macrocrysts). The crystal framework is permeated by interstitial glass (dark areas). d) Thin section image of a gabbroic nodule from Saxi. The framework comprises plagioclase macrocrysts with minor olivine macrocrysts. Clinopyroxene crystals are mostly found in glomerophyric clots in interstitial positions. e) Thin section image from Drekahraun. Note the lower abundance of macrocrysts compared to Brandur samples. Thin section images were

DOI: https://doi.org/10.2138/am-2021-7670. http://www.minsocam.org/

acquired with the use of a high-resolution scanner and the thin sections placed between two polarizing sheets to display the interference colors of different phases. plg: plagioclase; ol: olivine; cpx: clinopyroxene. gl: glass

Fig. 3. a) Core versus rim compositions of modeled olivine macrocrysts from all studied magmatic units. Brandur, Fontur and Saxi olivines have similar and narrow core compositions and more variable rim compositions. Þjórsárdalshraun, Drekahraun and Veiðivötn record distinct rim compositions with a narrow range, whereas olivine cores show a larger compositional range. Most macrocrysts plot below the black 1:1 line, meaning that they are normally zoned. b) Rhodes diagram to test for olivine-liquid equilibrium. Olivine in equilibrium with coexisting liquid compositions should fall in the grey field indicative of a $Kd_{(Fe\text{-}Mg)}^{ol\text{-}liq}$ = 0.30 ± 0.03 (Roeder and Emslie 1970). Rim compositions of the studied olivine macrocrysts are close to being in equilibrium with the carrier liquid. Colored bars depict 1σ compositional variability uncertainty of the carrier liquid of each sample, where the glass composition is taken as representative of the carrier liquid. The large variation of the Þjórsárdalshraun carrier liquid is due to its microcrystalline nature.

Fig. 4. Representative backscattered electron (BSE) images (a,d,g,j,m,p), concentration profiles with model fits (b, e, h, k, n, q) and stereographic plots (c, f, i, l, o, r) of studied olivine macrocrysts from all localities. White arrows in the BSE photos indicate the position of the analytical traverse. Black dashed lines indicate the assumed initial profile. Red lines are best fit models for the measured compositional gradient. For each macrocryst the calculated timescale (days) is also reported. The orientation of crystallographic axes with respect to the direction of the EPMA traverse (red cross) is shown in the stereographic plots. Analytical error of EPMA data is based on 2σ for multiple standard analyses.

Fig. 5. Fe-Mg diffusion modeling timescale results for a) Brandur, b) Fontur, c) Saxi, d) Þjórsárdalshraun, e) Drekahraun and f) Veiðivötn 1477. Early-Holocene units (Brandur, Fontur and Saxi tephra cones) record longer and more variable timescales up to 1300 days, compared to other magmatic units. Timescale uncertainties have been calculated following the procedure described by Kahl et al. (2015). Olivines found in the gabbroic nodules and in the tephra samples are shown with different markers. n=number of modeled olivine macrocrysts for each locality.

Fig. 6. Kernel density estimate plots with bandwidth 0.1, showing calculated timescales for a) early-Holocene units, b) middle-Holocene units and c) historical unit. Early-Holocene units record the largest timescale variation among all localities, with a main distribution peak between 200-400 days. n=number of olivine macrocrysts modeled for each locality.

Fig. 7. a) Olivine core compositions plotted versus melt inclusion (MI) OPAM equilibration pressures. Early-Holocene macrocrysts are separated into olivines from tephra samples (upwards-pointing triangles) and olivines from gabbroic nodule samples (inverted triangles). Most of the MIs are hosted in olivine macrocrysts from Brandur (n=10), Fontur (n=3) and Saxi (n=5). A statistically significant linear correlation (R^2=0.70) between MI OPAM pressure, MI composition and olivine Fo is observed among macrocrysts from early-Holocene units. As they move upwards in the crust, the composition of crystals and melts becomes more evolved, suggesting storage and evolution across a stacked-sills system. Error bar refers to the OPAM standard error of estimate (SSE=1.3 kbar). Grey symbols are olivine-hosted MIs from Caracciolo et al. (2020). b) Olivine diffusion timescales vs MI OPAM pressures within the same

macrocrysts. Olivines that have crystallized in deep-seated regions record similar timescales to olivines formed at mid-crustal levels. Symbols colored according to melt inclusion Mg#.

Fig. 8. Schematic cartoon (not to scale) summarizing processes operating underneath the Bárðarbunga-Veiðivötn volcanic system in the early-Holocene (a-b) and in the middle-Holocene to present time (c-d). Our observations suggest the presence of a multi-tiered magmatic system in which crystals are gradually transported to shallower levels and exposed to more evolved compositions. The main storage reservoir(s) is located at 7-10 km depth (Caracciolo et al. 2020). a) In the early-Holocene, the mid-crustal storage zone is composed of a packed and compact mush fabric, containing predominantly primitive crystals which are transferred throughout stacked-sills at different depths. b) Around 200-400 days before the eruption, relatively evolved melts located in the middle-crust intruded into the mushy reservoir(s), marking the onset of olivine equilibration. This intense melt injection, possibly triggered by rifting events and/or enhanced by increased early-postglacial melt production rates, caused loosening and mobilization of the packed mush pile(s). The incorporation of macrocrysts and crystalline gabbroic nodules in the carrier liquid and subsequent vertical transport occurred over long and variable timescales (~200-400 days). c) Macrocrysts are more evolved in composition and they are more likely to have formed at mid-crustal levels (1-4 kbar), with no evidences of deep-seated storage reservoirs (Caracciolo et al. 2020). Since the middle-Holocene, the mid-crustal storage reservoir(s) is composed of a less rigid mush fabric with relatively evolved crystals being more abundant compared to the early Holocene. d) Once evolved melt pocket(s) intruded the reservoir, the mush was quickly remobilized and macrocrysts ascended to the surface within short timescales (days up to a few months). Different color gradients of crystals and melt layers point out a variation of composition with time and

throughout the crust. However, different colors do not reflect real crystal or melt populations. ol: olivine; plg: plagioclase; cpx: clinopyroxene.

Fig. 9. Estimated timescales in the Bárðarbunga-Veiðivötn volcanic system for different eruptions as a function of time and macrocryst cargo. Subglacial and early-Holocene units record highly variable crystal mush disaggregation timescales with the most probable estimates on the order of a few months to one year. Subglacial and early-Holocene units have the largest macrocryst content (up to 45 vol %) among all studied localities. Middle-Holocene and historical units record narrow timescale variations in the range of a few months at most. These more recent magmatic units are associated with relatively small macrocryst load. The denser mush fabric associated with subglacial and early-Holocene units could be responsible for the observed longer timescales between melt injection, mush mobilization and eruption. Most probable timescales for the Skuggafjöll eruption are between 50 and 400 days. Data for Skuggafjöll are taken from Mutch et al. (2020) and Neave et al. (2014). Sku= Skuggafjöll, B=Brandur, F=Fontur, S=Saxi, Th= Þjórsárdalshraun, Dr= Drekahraun, V1477= Veiðivötn 1477.

Fig. 10. Compilation of crystal mush disaggregation to eruption timescales derived from modeling diffusive re-equilibration of compositional zoning in magmatic macrocrysts. We report all crystal mush disaggregation timescale ranges from Iceland (light green field) along with available literature data for mid-ocean ridge settings (light yellow field). In each case, the light-shaded bar represents the full range of calculated diffusion times while the inner black bar indicates the location of the most probable band in a KDE distribution within the time interval. Diffusion timescales modeled in this work are indicated

This is the peer-reviewed, final accepted version for American Mineralogist, published by the Mineralogical Society of America.
The published version is subject to change. Cite as Authors (Year) Title. American Mineralogist, in press.
DOI: https://doi.org/10.2138/am-2021-7670. http://www.minsocam.org/

with colored bars. Eruptions within the Bárðarbunga volcanic system are outlined by the black square and ordered according to time from subglacial to historical units. The volcanic eruptions are listed below the horizontal axis. Note that the timescale on the vertical axis is logarithmic. From left to right: Skuggafjöll (Mutch et al. 2020); Brandur, Fontur, Saxi, Þjórsárdalshraun, Drekahraun and Veiðivötn 1477 (this study); Holuhraun 2014-2015 (Hartley et al. 2018); Laki 1783-84 (Hartley et al. 2016); Eyjafjallajökull 500-720 ka (Nikkola et al. 2019); Eyjafjallajökull 2010 (Pankhurst et al. 2018); Serocki Volcano (Costa et al. 2010); Cost Rica Rift (Costa et al. 2010); East Pacific Rise 2005-06 (Moore et al. 2014). n_{ol} = number of olivine crystals modeled for diffusion kinetics; n_{plg} = number of plagioclase crystals modeled for diffusion kinetics. [a] Diffusion chronometry calculated with a different method: timescales are based on H^+ re-equilibration between plagioclase (n=70) and olivine-hosted (n=9) melt inclusions with a more hydrous melt. [b] Authors do not specify timescale ranges. For those eruptions, the interval between crystal mush disaggregation and eruption is ≤ 1.5 years (Serocki Volcano), <10 days (Costa Rica Rift) and <2 days (East Pacific Rise).

References 2:

References

Bjarnason, I. (2008) An Iceland hotspot saga. Jökull, 3–16.

Blundy, J., and Cashman, K. (2008) Petrologic reconstruction of magmatic system variables and processes. Reviews in Mineralogy and Geochemistry, 69, 179–239.

Caracciolo, A., Bali, E., Guðfinnsson, G.H., Kahl, M., Halldórsson, S.A., Hartley, M.E., and Gunnarsson, H. (2020) Temporal evolution of magma and crystal mush storage conditions in the Bárðarbunga-Veiðivötn volcanic system, Iceland. Lithos, 352–353.

Cashman, K. V., Sparks, R.S.J., and Blundy, J.D. (2017) Vertically extensive and unstable magmatic systems: A unified view of igneous processes. Science, 355, 1–9.

Chamberlain, K.J., Morgan, D.J., and Wilson, C.J.N. (2014) Timescales of mixing and mobilisation in the Bishop Tuff magma body: Perspectives from diffusion chronometry. Contributions to Mineralogy and Petrology, 168, 1–24.

Clark, A.M., and Long, J.V.P. (1971) Anisotropic diffusion of nickel in olivine. In Thomas Graham Memorial Symposium on Diffusion Proceses,Volume 2 pp. 511–521.

Coogan, L.A., Hain, A., Stahl, S., and Chakraborty, S. (2005) Experimental determination of the diffusion coefficient for calcium in olivine between 900°C and 1500°C. Geochimica et Cosmochimica Acta, 69, 3683–3694.

Cooper, K.M., and Kent, A.J.R. (2014) Rapid remobilization of magmatic crystals kept in cold storage. Nature, 506, 480–483.

Costa, F., and Chakraborty, S. (2004) Decadal time gaps between mafic intrusion and silicic eruption obtained from chemical zoning patterns in olivine. Earth and Planetary Science Letters, 227, 517–530.

Costa, F., and Morgan, D. (2010) Time Constraints from Chemical Equilibration in Magmatic Crystals, 125–159 p. Timescales of Magmatic Processes: From Core to Atmosphere.

Costa, F., Dohmen, R., and Chakraborty, S. (2008) Time Scales of Magmatic Processes from Modeling the Zoning Patterns of Crystals. Reviews in Mineralogy and Geochemistry, 69, 545–594.

Costa, F., Coogan, L.A., and Chakraborty, S. (2010) The time scales of magma mixing and mingling involving primitive melts and melt-mush interaction at mid-ocean ridges. Contributions to Mineralogy and Petrology, 159, 371–387.

Demouchy, S., Jacobsen, S.D., Gaillard, F., and Stem, C.R. (2006) Rapid magma ascent recorded by water diffusion profiles in mantle olivine. Geology, 34, 429–432.

Dohmen, R., Becker, H.W., and Chakraborty, S. (2007) Fe-Mg diffusion in olivine I: Experimental determination between 700 and 1,200°C as a function of composition, crystal orientation and oxygen fugacity. Physics and Chemistry of Minerals, 34, 389–407.

Dohmen, R., Faak, K., and Blundy, J.D. (2017) Chronometry and Speedometry of Magmatic Processes using Chemical Diffusion in Olivine, Plagioclase and Pyroxenes. Reviews in Mineralogy and Geochemistry, 83, 535–575.

Faak, K., Chakraborty, S., and Coogan, L.A. (2013) Mg in plagioclase: Experimental calibration of a new geothermometer and diffusion coefficients. Geochimica et Cosmochimica Acta, 123, 195–217.

Gee, M.A.M., Taylor, R.N., Thirlwall, M.F., and Murton, B.J. (1998) Glacioisostacy controls chemical and isotopic characteristics of tholeiites from the Reykjanes Peninsula , SW Iceland. Earth and Planetary Science Letters, 164, 1–5.

Ginibre, C., Wörner, G., and Kronz, A. (2007) Crystal Zoning as an Archive for Magma Evolution. Elements, 3, 261–266.

Haddadi, B., Sigmarsson, O., and Larsen, G. (2017) Magma storage beneath Grímsvötn volcano, Iceland, constrained by clinopyroxene-melt thermobarometry and volatiles in melt inclusions and groundmass glass. Journal of Geophysical Research: Solid Earth, 122, 6984–6997.

Halldórsson, S.A., Bali, E., Hartley, M.E., Neave, D.A., Peate, D.W., Guðfinnsson, G.H., Bindeman, I., Whitehouse, M.J., Riishuus, M.S., Pedersen, G.B.M., and others (2018) Petrology and geochemistry of the 2014–2015 Holuhraun eruption, central Iceland: compositional and mineralogical characteristics, temporal variability and magma storage. Contributions to Mineralogy and Petrology, 173, 1–25.

Hansen, H., Grönvold, K., 2000. Plagioclase ultraphyric basalts in Iceland : the mush of the rift. Journal of Volcanology and Geothermal Research 98, 1-32.

Hartley, M.E., Morgan, D.J., Maclennan, J., Edmonds, M., and Thordarson, T. (2016) Tracking timescales of short-term precursors to large basaltic fissure eruptions through Fe-Mg diffusion in olivine. Earth and

Planetary Science Letters, 439, 58–70.

Hartley, M.E., Bali, E., Maclennan, J., Neave, D.A., and Halldórsson, S.A. (2018) Melt inclusion constraints on petrogenesis of the 2014–2015 Holuhraun eruption, Iceland. Contributions to Mineralogy and Petrology, 173, 1–23.

Holzapfel, C., Chakraborty, S., Rubie, D.C., and Frost, D.J. (2007) Effect of pressure on Fe-Mg, Ni and Mn diffusion in (FexMg1-x)2SiO4olivine. Physics of the Earth and Planetary Interiors, 162, 186–198.

Kahl, M., Chakraborty, S., Costa, F., and Pompilio, M. (2011) Dynamic plumbing system beneath volcanoes revealed by kinetic modeling, and the connection to monitoring data: An example from Mt. Etna. Earth and Planetary Science Letters, 308, 11–22.

Kahl, M., Chakraborty, S., Costa, F., Pompilio, M., Liuzzo, M., and Viccaro, M. (2013) Compositionally zoned crystals and real-time degassing data reveal changes in magma transfer dynamics during the 2006 summit eruptive episodes of Mt. Etna. Bulletin of Volcanology, 75, 1–14.

Kahl, M., Chakraborty, S., Pompilio, M., and Costa, F. (2015) Constraints on the nature and evolution of the magma plumbing system of Mt. Etna volcano (1991-2008) from a combined thermodynamic and kinetic modelling of the compositional record of minerals. Journal of Petrology, 56, 2025–2068.

Kahl, M., Viccaro, M., Ubide, T., Morgan, D.J., and Dingwell, D.B. (2017) A branched magma feeder system during the 1669 eruption of Mt Etna: Evidence from a time-integrated study of zoned olivine phenocryst populations. Journal of Petrology, 58, 443–472.

Kelemen, P.B., Koga, K., and Shimizu, N. (1997) Origin of gabbro sills in the Moho transition zone of the Oman ophiolite: Implications for magma transport in the oceanic lower crust. Journal of Geophysical Research: Solid Earth, 102, 475–488

Kress, V.C., and Carmichael, I.S.E. (1991) The compressibility of silicate liquids containing Fe2O3 and the effect of composition, temperature, oxygen fugacity and pressure on their redox states. Contributions to Mineralogy and Petrology, 108, 82–92.

Larsen, G., and Guðmundsson, M.T. (2014) Volcanic system : Bárðarbunga system. Catalogue of Icelandic

Volcanoes, 1–11.

Le Breton, E., Dauteuil, O., and Biessy, G. (2016) Post-glacial rebound of Iceland during the Holocene. Journal of the Geological Society, London, 167, 417–432.

Maclennan, J. (2008) Concurrent mixing and cooling of melts under Iceland. Journal of Petrology, 49, 1931–1953.

Maclennan, J. (2019) Mafic tiers and transient mushes: evidence from Iceland. Philosophical Transactions of the Royal Society A, 377, 1–20.

Martin, V.M., Morgan, D.J., Jerram, D.A., Caddick, M.J., Prior, D.J., and Davidson, J.P. (2008) Bang! Month-scale eruption triggering at santorini volcano. Science, 321, 1178.

Mattsson, H.B., and Oskarsson, N. (2005) Petrogenesis of alkaline basalts at the tip of a propagating rift: Evidence from the Heimaey volcanic centre, south Iceland. Journal of Volcanology and Geothermal Research, 147, 245–267.

Moore, A., Coogan, L.A., Costa, F., and Perfit, M.R. (2014) Primitive melt replenishment and crystal-mush disaggregation in the weeks preceding the 2005-2006 eruption 9°50' N, EPR. Earth and Planetary Science Letters, 403, 15–26.

Mutch, E., Maclennan, J., Shorttle, O., Rudge, J., and Neave, D. (2020) DFENS: Diffusion chronometry using Finite Elements and Nested Sampling. Earth and Space Science Open Archive.

Mutch, Euan J F, Maclennan, J., Holland, T.J.B., and Buisman, I. (2019b) Millennial storage of near-Moho magma. Science, 264, 260–264.

Mutch, Euan J. F., Maclennan, J., Shorttle, O., Edmonds, M., and Rudge, J.F. (2019a) Rapid transcrustal magma movement under Iceland. Nature Geoscience.

Neave, D.A., and Putirka, K.D. (2017) A new clinopyroxene-liquid barometer , and implications for magma storage pressures under Icelandic rift zones. American Mineralogist, 102, 777–794.

Neave, D.A., Passmore, E., Maclennan, J., Fitton, G., and Thordarson, T. (2013) Crystal-melt relationships and the record of deep mixing and crystallization in the AD 1783 Laki eruption, Iceland. Journal of Petrology, 54, 1661–1690.

Neave, D.A., Maclennan, J., Hartley, M.E., Edmonds, M., and Thordarson, T. (2014) Crystal storage and transfer in basaltic systems: The skuggafjoll eruption, Iceland. Journal of Petrology, 55, 2311_2346.

Neave, D.A., Maclennan, J., Thordarson, T., and Hartley, M.E. (2015) The evolution and storage of primitive melts in the Eastern Volcanic Zone of Iceland: the 10 ka Grímsvötn tephra series (i.e. the Saksunarvatn ash). Contributions to Mineralogy and Petrology, 170, 1–23.

Newcombe, M.E., Fabbrizio, A., Zhang, Y., Ma, C., Le Voyer, M., Guan, Y., Eiler, J.M., Saal, A.E., and Stolper, E.M. (2014) Chemical zonation in olivine-hosted melt inclusions. Contributions to Mineralogy and Petrology, 168, 1–26.

Nikkola, P., Bali, E., Kahl, M., van der Meer, Q.H.A., Rämö, O.T., Guðfinnsson, G.H., and Thordarson, T. (2019) Mid-crustal storage and crystallization of Eyjafjallajökull. Jökull, 69, 77–96.

Pankhurst, M.J., Dobson, K.J., Morgan, D.J., Loughlin, S.C., Thordarson, T.H., Lee, P.D., and Courtois, L. (2014) Technical note monitoring the magmas fuellingvolcanic eruptions in near-real-time using x-ray micro-computed tomography. Journal of Petrology, 55, 671–684.

Pankhurst, M.J., Morgan, D.J., Thordarson, T., and Loughlin, S.C. (2018) Magmatic crystal records in time, space, and process, causatively linked with volcanic unrest. Earth and Planetary Science Letters, 493, 231–241.

Petry, C., Chakraborty, S., and Palme, H. (2004) Experimental determination of Ni diffusion coefficients in olivine and their dependence on temperature, composition, oxygen fugacity, and crystallographic orientation. Geochimica et Cosmochimica Acta, 68, 4179–4188.

Pinton, A., Giordano, G., Speranza, F., and Thordarson, T. (2018) Paleomagnetism of Holocene lava flows from the Reykjanes Peninsula and the Tungnaá lava sequence (Iceland): implications for flow correlation and ages. Bulletin of Volcanology, 80, 1–19.

Rae, A.S.P., Edmonds, M., Maclennan, J., Morgan, D., Houghton, B., Hartley, M.E., and Sides, I. (2016) Time scales of magma transport and mixing at Kīlauea Volcano, Hawai'i. Geology, 44, 463–466.

Rasmussen, D.J., Plank, T.A., Roman, D.C., Power, J.A., Bodnar, R.J., and Hauri, E.H. (2018) When does eruption run-up begin? Multidisciplinary insight from the 1999 eruption of Shishaldin volcano. Earth and Planetary Science Letters, 486, 1–14.

Roeder, P.L., and Emslie, R.F. (1970) Olivine-liquid equilibrium. Contribution to MIneralogy and Petrology, 29, 275–289.

Ruprecht, P., and Cooper, K.M. (2012) Integrating the uranium-series and elemental diffusion geochronometers in mixed magmas from Volcán Quizapu, Central Chile. Journal of Petrology, 53, 841–871.

Ruprecht, P., and Plank, T. (2013) Feeding andesitic eruptions with a high-speed connection from the mantle. Nature, 500, 68–72.

Shea, T., Costa, F., D. Krimer, and Hammer, J.E. (2015) Accuracy of timescales retrieved from diffusion modeling in olivine : A 3D perspective †, 100, 2026–2042.

Sigmundsson, F., Hreinsdóttir, S., Hooper, A., Árnadóttir, T., Pedersen, R., Roberts, M.J., Óskarsson, N., Auriac, A., Decriem, J., Einarsson, P., and others (2010) Intrusion triggering of the 2010 Eyjafjallajökull explosive eruption. Nature, 468, 426–432.

Sigmundsson, F., Pinel, V., Grapenthin, R., Hooper, A., Halldórsson, S.A., Einarsson, P., Ófeigsson, B.G., Heimisson, E.R., Jónsdóttir, K., Gudmundsson, M.T., and others (2020) Unexpected large eruptions from buoyant magma bodies within viscoelastic crust. Nature Communications, 11, 1–11.

Sinton, J., Grönvold, K., and Sæmundsson, K. (2005) Postglacial eruptive history of the Western Volcanic Zone, Iceland. Geochemistry, Geophysics, Geosystems, 6, 1–34.

Sio, C.K.I., Dauphas, N., Teng, F.Z., Chaussidon, M., Helz, R.T., and Roskosz, M. (2013) Discerning crystal growth from diffusion profiles in zoned olivine by in situ Mg-Fe isotopic analyses. Geochimica et Cosmochimica Acta, 123, 302–321.

Sparks, R.S.J., and Sigurdsson, H. (1977) Magma mixing: a mechanism for triggering acid explosive eruptions. Nature, 267, 315–318.

Streck, M.J. (2008) Mineral textures and zoning as evidence for open system processes. Reviews in Mineralogy and Geochemistry, 69, 595–622.

Thomson, A., and Maclennan, J. (2013) The distribution of olivine compositions in icelandic basalts and picrites. Journal of Petrology, 54, 745–768.

Thordarson, T., and Larsen, G. (2007) Volcanism in Iceland in historical time: Volcano types, eruption styles and eruptive history. Journal of Geodynamics, 43, 118–152.

Turner, S., and Costa, F. (2007) Measuring timescales of magmatic evolution. Elements, 3, 267–272.

Viccaro, M., Giuffrida, M., Nicotra, E., and Cristofolini, R. (2016) Timescales of magma storage and migration recorded by olivine crystals in basalts of the March-April 2010 eruption at Eyjafjallajökull volcano, Iceland. American Mineralogist, 101, 222–230.

Wanless, V.D., and Shaw, A.M. (2012) Lower crustal crystallization and melt evolution at mid-ocean ridges. Nature Geoscience, 5, 651–655.

Yang, H.-J., Kinzler, R.J., and Grove, T.L. (1996) Experiments and models of anhydrous, basaltic olivine-plagioclase-augite saturated melts from 0.001 to 10 kbar. Contributions to Mineralogy and Petrology, 124, 1–18.

Zellmer, G.F., Dulski, P., Iizuka, Y., and Perfit, M.R. (2012) Rates and processes of crystallization in on-axis and off-axis MOR basaltic melts. Lithos, 154, 1–15.

Figure 1

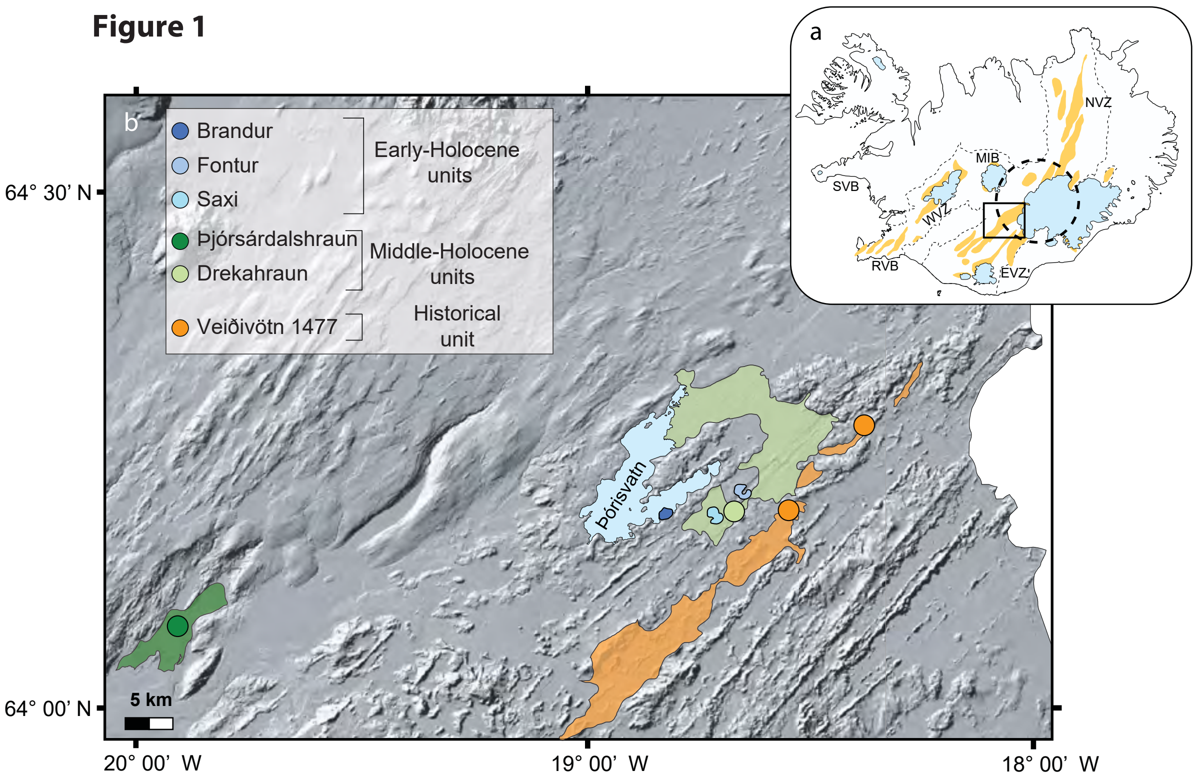

a
NVZ
MIB
SVB
WVZ
RVB
EVZ
b
Brandur
Fontur
Saxi
Early-Holocene units
Þjórsárdalshraun
Drekahraun
Middle-Holocene units
Veiðivötn 1477
Historical unit
Þórisvatn
5 km
64° 30' N
64° 00' N
20° 00' W
19° 00' W
18° 00' W

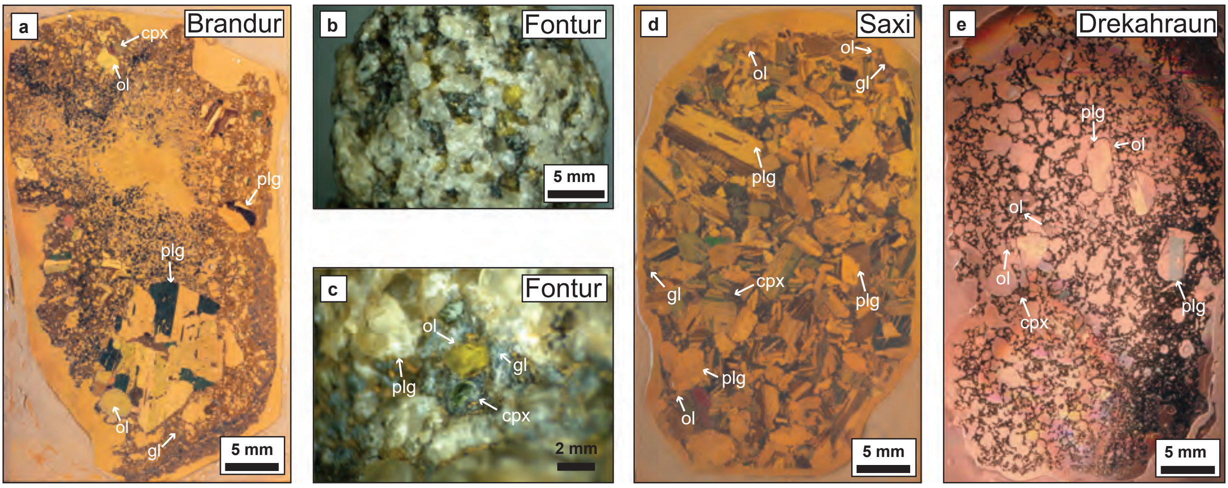
a
Brandur
cpx
ol
plg
plg
ol
gl
5 mm
b
Fontur
5 mm
c
Fontur
ol
plg
gl
cpx
2 mm
d
Saxi
ol
ol
gl
plg
gl
cpx
plg
plg
ol
5 mm
e
Drekahraun
plg
ol
ol
ol
cpx
plg
5 mm

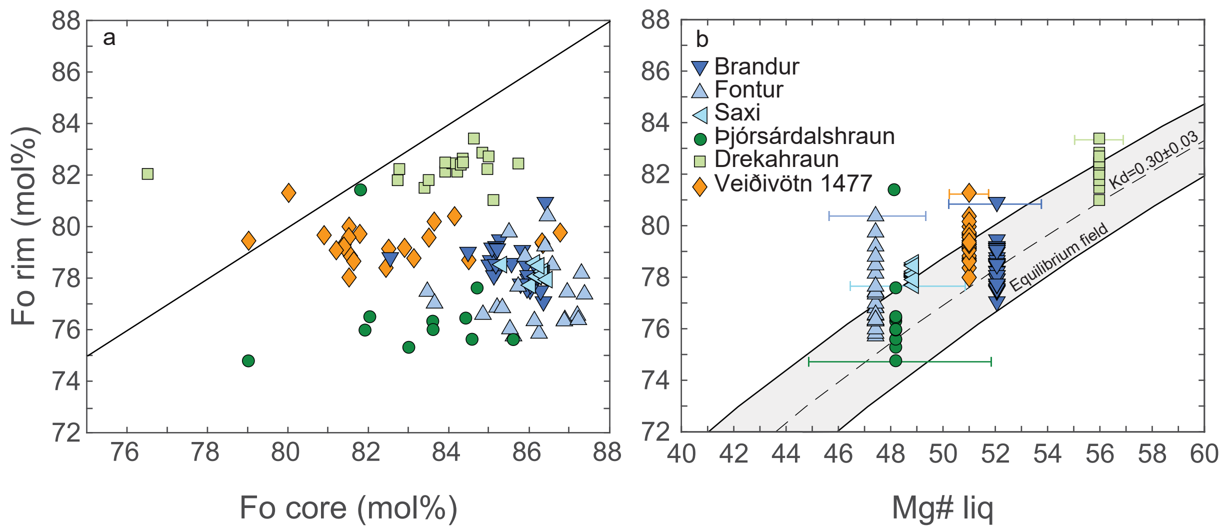

a
Fo rim (mol%)
Fo core (mol%)
b
Brandur
Fontur
Saxi
Þjórsárdalshraun
Drekahraun
Veiðivötn 1477
Kd=0.30±0.03
Equilibrium field
Mg# liq

Figure 3

Figure 4

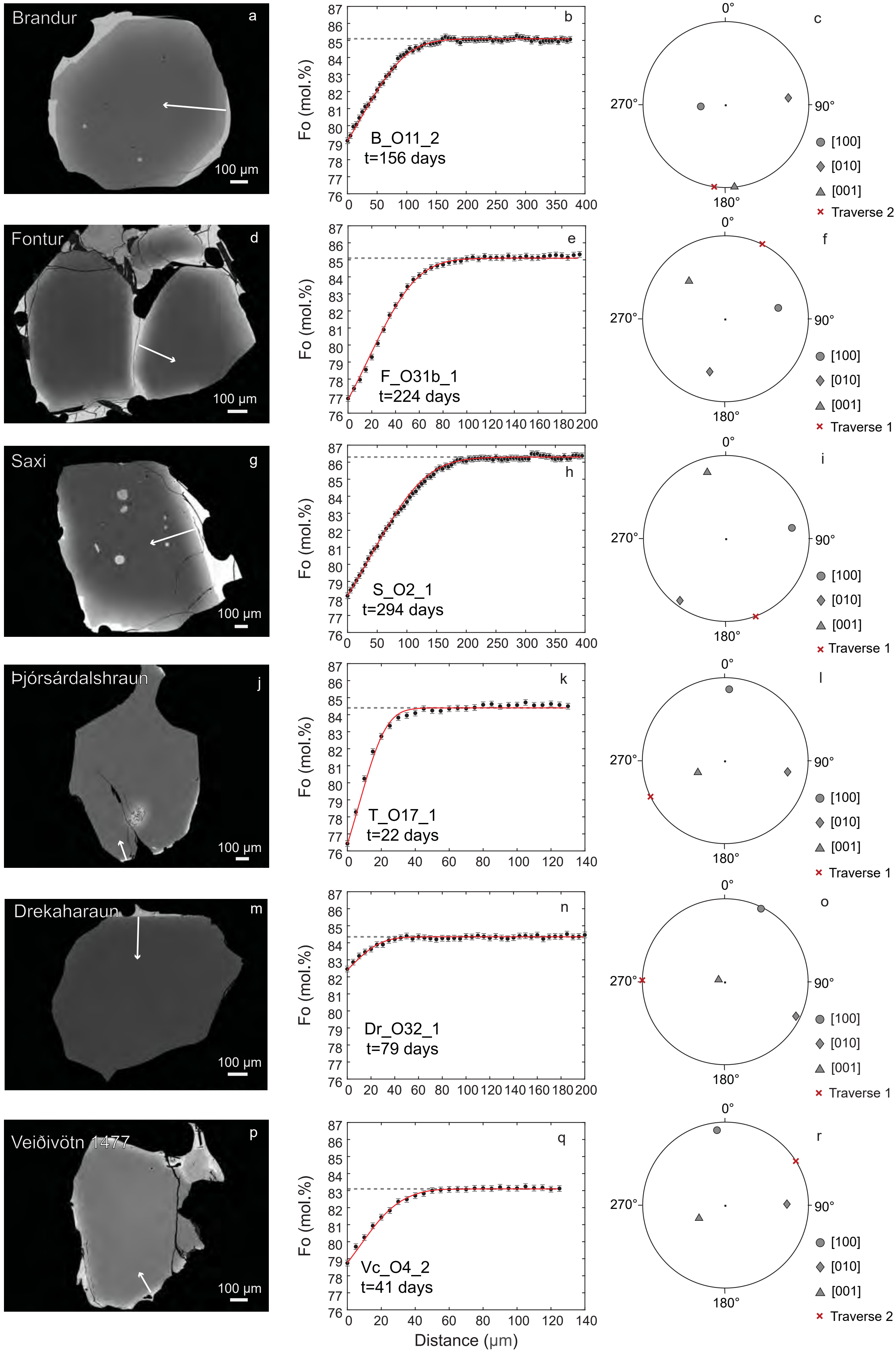

Brandur
a
100 μm
b
B_O11_2
t=156 days
Fo (mol.%)
c
0°
90°
180°
270°
[100]
[010]
[001]
Traverse 2
Fontur
d
100 μm
e
F_O31b_1
t=224 days
f
Traverse 1
Saxi
g
100 μm
h
S_O2_1
t=294 days
i
Traverse 1
Þjórsárdalshraun
j
100 μm
k
T_O17_1
t=22 days
l
Traverse 1
Drekaharaun
m
100 μm
n
Dr_O32_1
t=79 days
o
Traverse 1
Veiðivötn 1477
p
100 μm
q
Vc_O4_2
t=41 days
r
Traverse 2
Distance (μm)

Figure 5

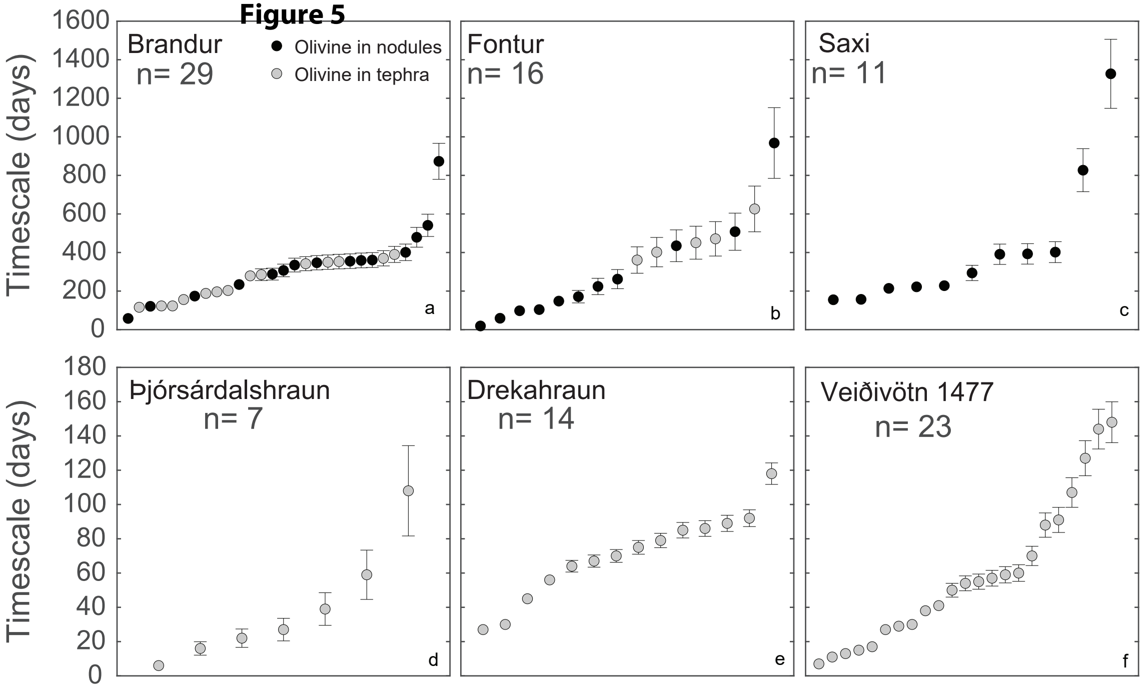

Brandur
n= 29
Olivine in nodules
Olivine in tephra
Fontur
n= 16
Saxi
n= 11
Þjórsárdalshraun
n= 7
Drekahraun
n= 14
Veiðivötn 1477
n= 23
Timescale (days)
a
b
c
d
e
f

Figure 6

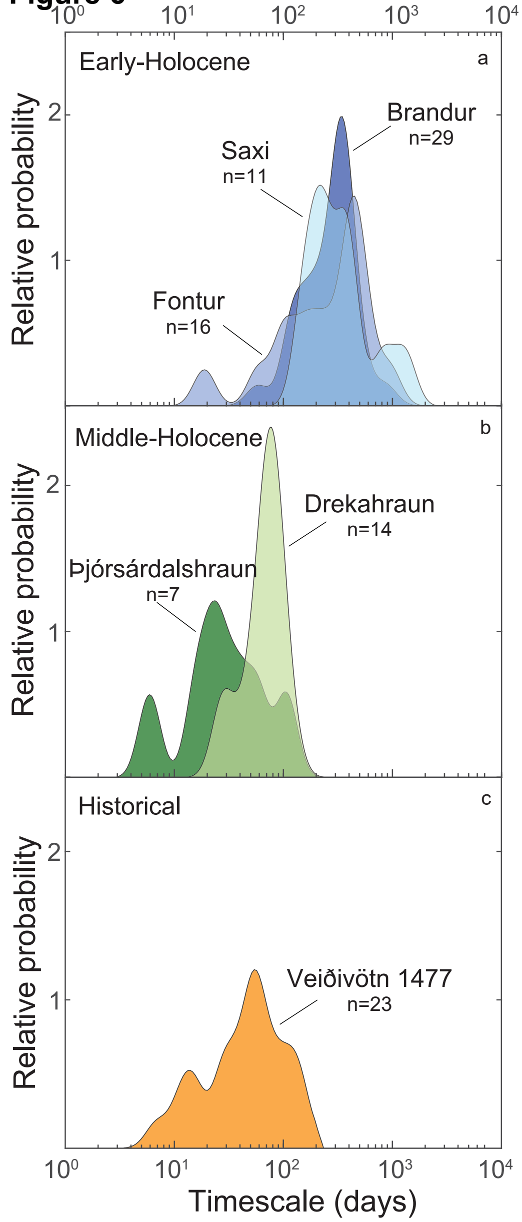

Early-Holocene
a
Brandur
n=29
Saxi
n=11
Fontur
n=16
Relative probability
Middle-Holocene
b
Drekahraun
n=14
Þjórsárdalshraun
n=7
Relative probability
Historical
c
Veiðivötn 1477
n=23
Relative probability
Timescale (days)

Figure 7

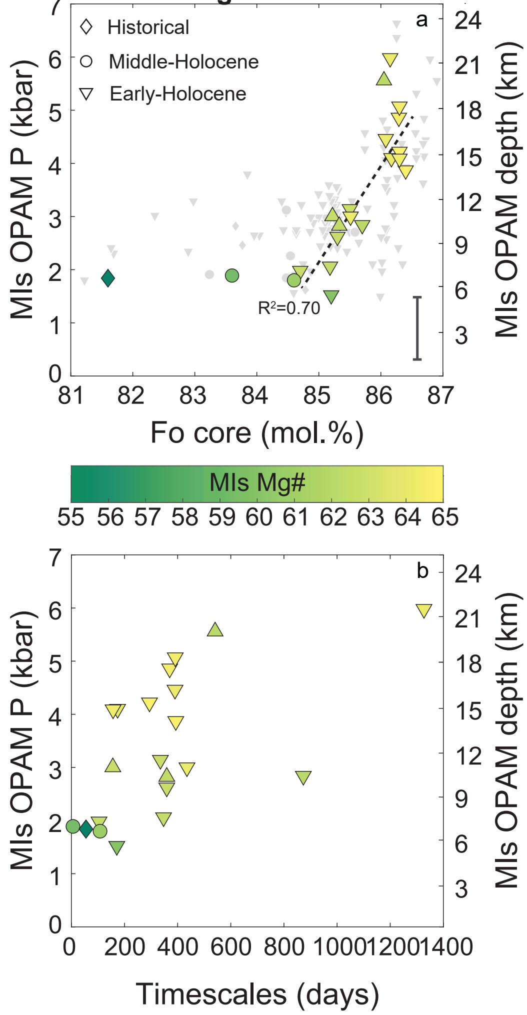

Historical
Middle-Holocene
Early-Holocene
a
MIs OPAM P (kbar)
MIs OPAM depth (km)
R²=0.70
Fo core (mol.%)
MIs Mg#
b
MIs OPAM P (kbar)
MIs OPAM depth (km)
Timescales (days)

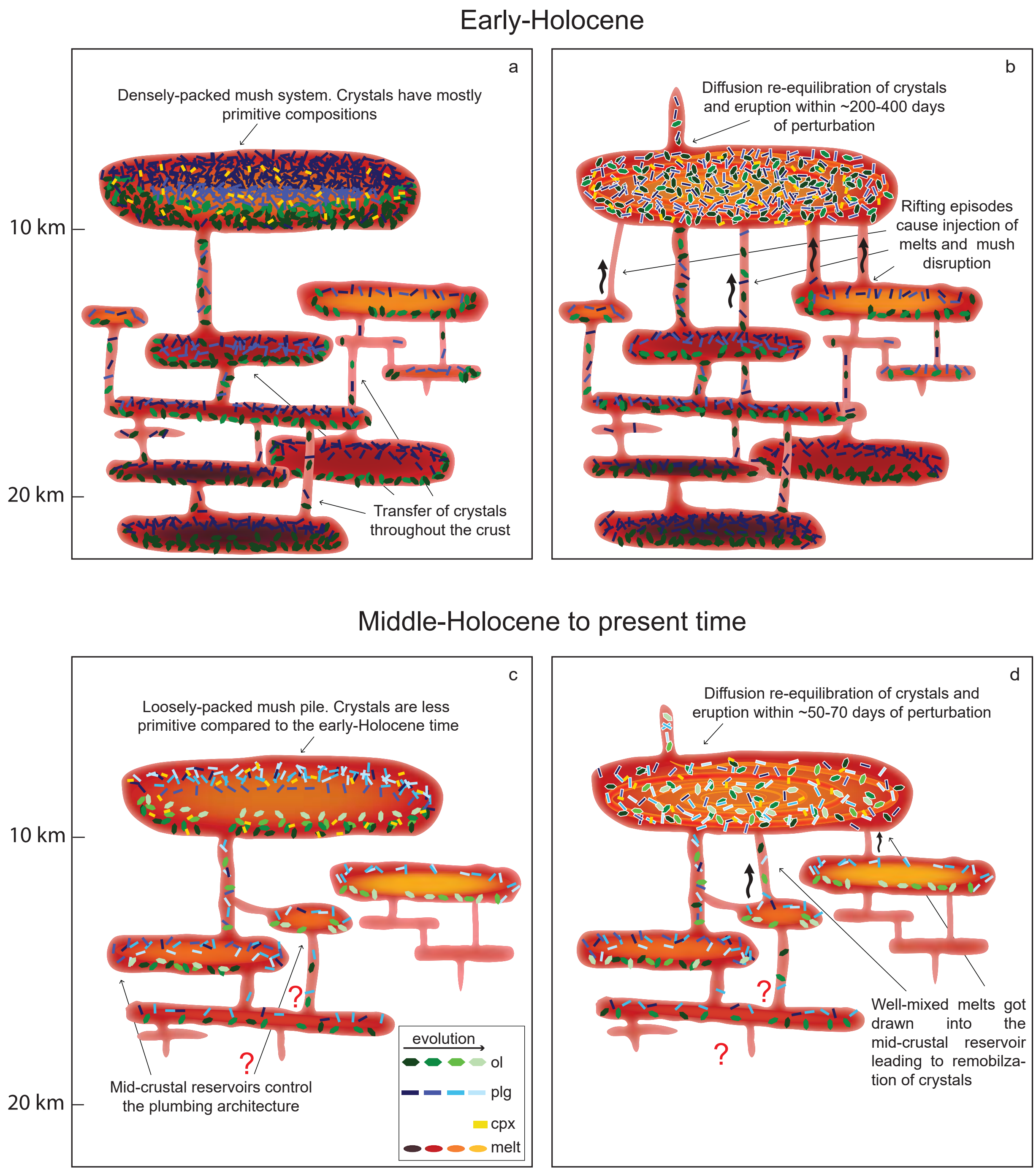
Early-Holocene
a
Densely-packed mush system. Crystals have mostly primitive compositions
10 km
20 km
Transfer of crystals throughout the crust
b
Diffusion re-equilibration of crystals and eruption within ~200-400 days of perturbation
Rifting episodes cause injection of melts and mush disruption
Middle-Holocene to present time
c
Loosely-packed mush pile. Crystals are less primitive compared to the early-Holocene time
10 km
20 km
?
?
Mid-crustal reservoirs control the plumbing architecture
evolution
ol
plg
cpx
melt
d
Diffusion re-equilibration of crystals and eruption within ~50-70 days of perturbation
?
?
Well-mixed melts got drawn into the mid-crustal reservoir leading to remobilza-tion of crystals

Figure 8

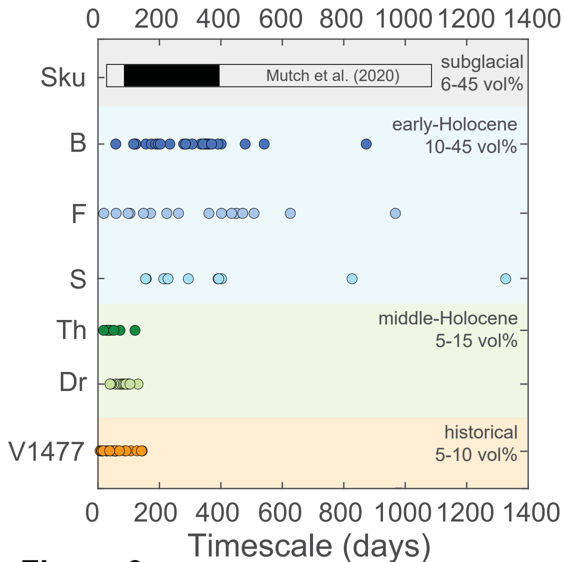

0 200 400 600 800 1000 1200 1400
Sku
Mutch et al. (2020)
subglacial
6-45 vol%
B
early-Holocene
10-45 vol%
F
S
Th
middle-Holocene
5-15 vol%
Dr
V1477
historical
5-10 vol%
0 200 400 600 800 1000 1200 1400
Timescale (days)

Figure 9

Figure 10

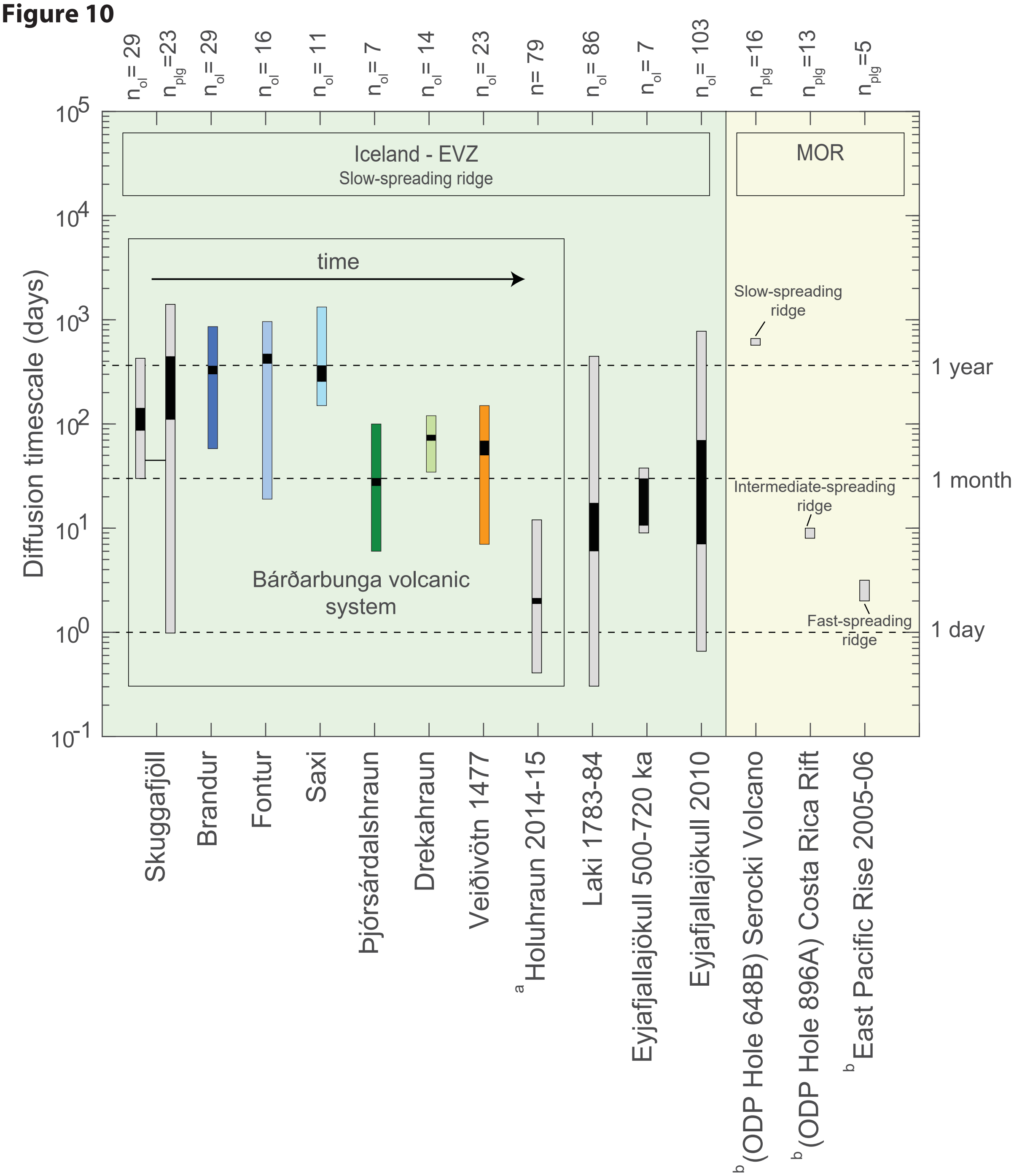

n_{ol}= 29
n_{plg}=23
n_{ol}= 29
n_{ol}= 16
n_{ol}= 11
n_{ol}= 7
n_{ol}= 14
n_{ol}= 23
n= 79
n_{ol}= 86
n_{ol}= 7
n_{ol}= 103
n_{plg}=16
n_{plg}=13
n_{plg}=5
Iceland - EVZ
Slow-spreading ridge
MOR
time
Bárðarbunga volcanic system
Slow-spreading ridge
Intermediate-spreading ridge
Fast-spreading ridge
1 year
1 month
1 day
Diffusion timescale (days)
10^5
10^4
10^3
10^2
10^1
10^0
10^{-1}
Skuggafjöll
Brandur
Fontur
Saxi
Þjórsárdalshraun
Drekahraun
Veiðivötn 1477
[a] Holuhraun 2014-15
Laki 1783-84
Eyjafjallajökull 500-720 ka
Eyjafjallajökull 2010
[b] (ODP Hole 648B) Serocki Volcano
[b] (ODP Hole 896A) Costa Rica Rift
[b] East Pacific Rise 2005-06

Table 1. Number of olivine crystals, chemical profiles and timescale (days) result for each magmatic unit.

Unit	Age	Olivine grains	Chemical profiles	Modelled olivines	Timescale		Temperature*		Pressure*	
		n	*n*	*n*	*average*	*st.dev.*	*Mean*	*σ*	*Mean*	*σ*
Brandur	Early-Holocene	31	44	29	300	158	1170	4	2.2	0.7
Fontur	Early-Holocene	21	31	16	332	241	1161	7	2.2	0.6
Saxi	Early-Holocene	13	13	11	419	339	1163	5	2.3	0.7
Þjórsárdalshraun	Middle-Holocene	11	16	7	40	32	1160	9	1.9	0.7
Drekahraun	Middle-Holocene	19	27	14	70	24	1174	2	2.6	0.8
Veiðivötn 1477	1477 AD	26	42	23	58	41	1167	3	1.9	0.6

*Modelling input pressure (kbar) and temperature (°C) data from Caracciolo et al. (2020)